

Searching for the Kardar-Parisi-Zhang phase in microcavity polaritons

A. Ferrier,¹ A. Zamora,¹ G. Dagvadorj,¹ and M. H. Szymaska¹

¹*Department of Physics and Astronomy, University College London, Gower Street, London, WC1E 6BT, United Kingdom*

Recent analytical work has shown that, at certain values of the external pump, the optical parametric oscillator (OPO) regime of microcavity polaritons may provide a realisation of Kardar-Parisi-Zhang (KPZ) physics in 2D. Here, we verify this by solving the full microscopic model numerically using the truncated Wigner method, and studying the first order spatial correlations. For the predicted pump strengths, these correlations decay much faster and, perpendicular to the pump, fit closely to the stretched exponential form predicted by the KPZ equation, in contrast to the usual algebraic decay. This strongly indicates the viability of observing KPZ behaviour in future polariton OPO experiments.

The Kardar-Parisi-Zhang (KPZ) universality class offers a description of the long range behaviour in a wide variety of non-equilibrium systems. Originally conceived as a model of growing surfaces [1], the KPZ universality has since been found to encompass a plethora of physical realisations, including growing bacterial colonies [2–4], burning paper [5–7], and growing interfaces in liquid crystals [8–10]. Generally, however, most of these have been limited to one dimension, especially with regards to actual experiments.

One possible candidate for realising KPZ physics in both 1D and 2D, which has drawn a significant amount of theoretical attention, is the phase dynamics of polariton condensates in semiconductor microcavities [11–20]. In addition to potentially being able to provide a much sought after experimental platform for investigating the 2D KPZ universality class, due to the phase being a compact variable these systems also offer a window into an array of interesting new physics regarding the dynamics of vortices in the phase under the KPZ equation [15, 16, 21–23]. However, a consistent barrier has arisen in terms of the viability of reproducing these results in experiments, in that the length scales at which signs of KPZ are expected are unrealistically large compared to typical microcavities; this explains why previous numerical and experimental studies have only observed behaviour analogous to equilibrium physics [24, 25].

A potential way around this lies in an alternative regime of the microcavity polariton system, the optical parametric oscillator (OPO) regime. Here, rather than having a single condensate occupied by an incoherent drive, a coherently driven mode, the pump, scatters to occupy two other modes, referred to as the signal and idler (see Fig. 1). Recent work has shown [26] that not only does the OPO regime map similarly to a KPZ equation in the long range limit, with the relevant variable being the free phase difference between the signal and idler modes, but it is also highly tunable by varying the strength of the coherent drive, even leading to a small window in pump strength where the KPZ behaviour should become observable at all length scales.

While that analytical study indicates a promising

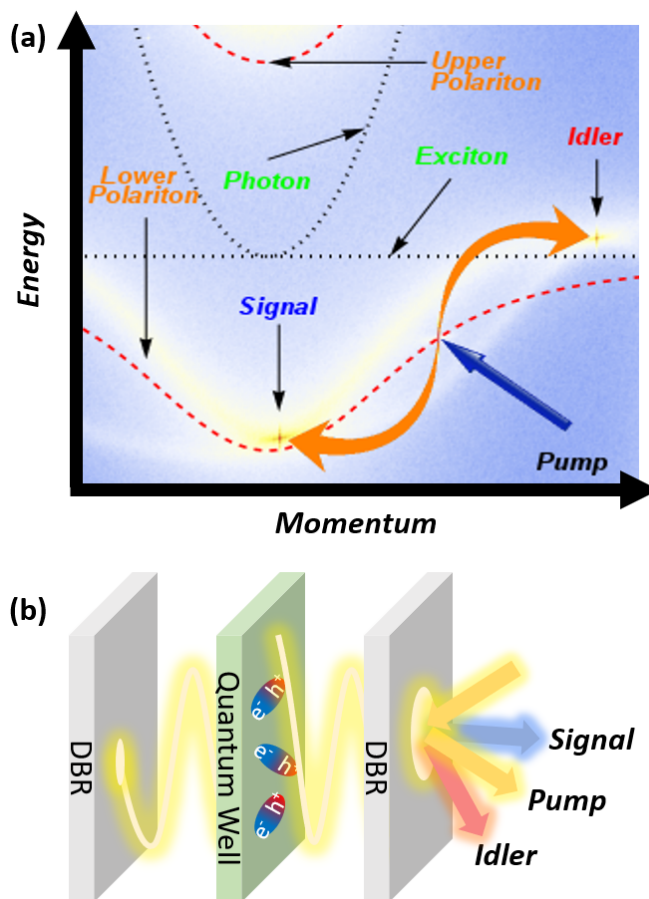


FIG. 1. Polaritons in semiconductor microcavities in the OPO regime. (a) Typical spectrum of OPO showing signal, pump and idler modes on the lower polariton branch. (b) Sketch of the system: External laser drives the pump mode, which then scatters to occupy the signal and idler.

direction for the possibility of observing 2D KPZ physics in polariton experiments, there still is a number of open questions that remain to be investigated to prove the viability of experimentally reproducing this behaviour. Specifically, the analysis in [26] involves a number of approximations that do not necessarily hold true in actual

systems. Firstly, that a strictly three mode (pump, signal, idler) model is considered, while in actual polariton OPO additional satellite states can also become relevant [27, 28]. Secondly, that density fluctuations, which are completely neglected in the long range limit when mapping to the KPZ equation, may still be a relevant factor in real finite size systems or when satellite states are included, leading to, for example, spatially non-uniform condensates, pattern formation or time-dependent solutions. As such, to address these questions, we now investigate the polariton OPO using full multimode stochastic simulations, which are not restricted by those approximations, to see if the signatures of the KPZ universality still appear when the pump strength is tuned to within the window found analytically. Observing the predicted behaviour in this sort of numerical analysis should open the way to its replication in actual experiments, and hence the use of the OPO regime of polaritons in semiconductor microcavities as an experimental platform for exploring KPZ physics in 2D.

Truncated Wigner Method. As illustrated by the spectrum in Fig. 1 (a), strong coupling between the cavity photons and quantum well excitons in semiconductor microcavities leads to two branches of polaritons – upper and lower. Since the OPO regime is achieved by coherently driving the lower polariton branch, we neglect the upper polariton branch that will have negligible occupation, and consider a model with only the lower polaritons. The lower polaritons have a non-quadratic dispersion given by $\omega_{lp}(\mathbf{k}) = \frac{1}{2} \left(\omega_c(\mathbf{k}) + \omega_x - \sqrt{(\omega_c(\mathbf{k}) - \omega_x)^2 + \Omega_R^2} \right)$, with $\omega_c(\mathbf{k})$ being the (quadratic) bare cavity photon dispersion, ω_x the exciton dispersion, which is approximately flat due its much larger mass, and Ω_R the Rabi frequency of exciton-photon coupling [29].

To study the system fully, we use stochastic simulations based on the truncated Wigner approximation (TWA) [30]. Unlike the three mode model of OPO used for analytical calculations, our numerical method considers the full two dimensional multimode lower polariton field, which includes fluctuations in both density and phase, represented by a stochastic complex number field $\Psi(\mathbf{x}, t)$, from which physical observables such as density and correlation functions can be calculated by appropriate averages over stochastic realisations. Considering the evolution of the Wigner quasiprobability distribution and truncating the third order derivative terms, reducing it to the form of a Fokker-Planck equation, leads to the following equation for trajectories of the stochastic complex number field $\Psi(\mathbf{x}, t)$:

$$\frac{\partial \Psi(\mathbf{x}, t)}{\partial t} = -iH\Psi(\mathbf{x}, t) + iF_p(\mathbf{x}, t) + \sqrt{\frac{\kappa}{dV}}\Gamma(\mathbf{x}, t), \quad (1)$$

with the differential operator H defined as

$$H = \omega_{lp}(-i\nabla) - i\kappa + g \left(|\Psi(\mathbf{x}, t)|^2 - \frac{1}{dV} \right),$$

where g is the polariton-polariton interaction strength, which we approximate as being momentum independent [27], κ is the polariton decay rate, and $F_p(\mathbf{x}, t) = f_p e^{i(k_p x - \omega_p t)}$ is a coherent drive at momentum k_p and frequency ω_p . $\Gamma(\mathbf{x}, t)$ is a zero mean complex Wiener noise with $\langle \Gamma^*(\mathbf{x}, t) \Gamma(\mathbf{x}', t') \rangle = \delta_{\mathbf{x}, \mathbf{x}'} \delta(t - t')$. Results of the TWA include all classical fluctuations and up to second order in quantum fluctuations [31], but neglect higher order quantum effects which are discarded by the truncation. These higher order effects, however, become relevant only for average mode occupations much smaller than one, which is not the case here. The area element $dV = a^2$ of the grid used to discretise space for numerical integration, where a is the lattice spacing of this grid, plays a role in determining the validity of this approximation. The TWA is appropriate under the condition that $\kappa \gg \frac{g}{dV}$. It then becomes important to chose a to be sufficiently small to maximise the accuracy of the integration with respect to the continuum limit, while still leaving it large enough to not go beyond the validity of the TWA.

All physical quantities will be expressed in units derived from the parameters of the system: times are expressed in units of $2/\Omega_R$, lengths in units of $\sqrt{\hbar/(\Omega_R m_c)}$, and energies in $\hbar\Omega_R/2$, where m_c is the effective mass of photons in the cavity. In these units, the values of the other parameters are $g = 0.00118$, $\kappa = 0.045$, with the drive on resonance with the lower polariton dispersion at $k_p = 1.4$, $\omega_p = -0.42$. We choose our energy scale, and the exciton-photon detuning, such that $\omega_x = \omega_c(0) = 0$. We consider a square area with side length $2L = 422.17544$, which is simulated on a $N \times N = 512 \times 512$ point grid, giving $a = 0.8246$ ($dV = 0.6799$). It should be noted that for these parameters, the upper and lower OPO thresholds occur at $f_p = 0.053$ and $f_p = 0.0135$ respectively [27].

Physical observables are calculated within the TWA using the relation that averages over the Wigner distribution (i.e. over stochastic realisations of our simulation) of products of the phase space variables correspond to quantum mechanical averages of the symmetrically ordered products of the relevant operators. Of particular interest in this work is the first order spatial correlation

$$g^{(1)}(\mathbf{r}) = \frac{\langle \Psi^*(\mathbf{R} + \mathbf{r}, t) \Psi(\mathbf{R}, t) \rangle - \frac{\delta_{\mathbf{r}, \mathbf{0}}}{2dV}}{\langle \Psi^*(\mathbf{R}, t) \Psi(\mathbf{R}, t) \rangle - \frac{1}{2dV}}, \quad (2)$$

where averages are taken over both stochastic realisations and the auxiliary position \mathbf{R} . By also using the properties of the Fourier transform, this can be efficiently

calculated in momentum space as:

$$g^{(1)}(\mathbf{r}) = \frac{\langle \Psi^*(\mathbf{k}, t) \Psi(\mathbf{k}, t) e^{i\mathbf{k}\cdot\mathbf{r}} \rangle - \frac{\delta_{\mathbf{r},0}}{2}}{\langle \Psi^*(\mathbf{k}, t) \Psi(\mathbf{k}, t) \rangle - \frac{1}{2}}, \quad (3)$$

where $\Psi(\mathbf{k}, t)$ represents the 2D Fourier transform of the stochastic complex number field $\Psi(\mathbf{x}, t)$, and $\langle \dots \rangle$ here represents averaging over both stochastic realisations and the momentum \mathbf{k} . Since we are interested in the OPO regime and want to consider the signal mode, we filter in momentum space, ultimately only considering \mathbf{k} within a square in momentum space of side length $(k_p - k_s)$ centred on the maximum of the signal mode at $\mathbf{k} = (k_s, 0)$. We will label the resulting momentum-filtered signal field in *real* space as $\Psi_s(\mathbf{x}, t)$, with $g_s^{(1)}(\mathbf{r})$ being its first order spatial correlation function calculated as described above when only including momenta within the filter.

Expected Signatures of KPZ physics in polariton OPO. In common theoretical descriptions, the polariton OPO system is approximated as consisting of three main modes: the pump mode, which is driven directly by an external laser, and the signal and idler modes, which become occupied by the parametric scattering of polaritons from the pump mode. In previous work [26], it was shown that the system of equations for the three modes reduces to an anisotropic KPZ equation (Eq. 4) for the Goldstone mode θ , the relative phase between the signal and idler modes, in the long range limit:

$$\partial_t \theta = D_x \partial_x^2 \theta + D_y \partial_y^2 \theta + \frac{\lambda_x}{2} (\partial_x \theta)^2 + \frac{\lambda_y}{2} (\partial_y \theta)^2 + \xi, \quad (4)$$

where $\xi(\mathbf{r}, t)$ is Gaussian noise with $\langle \xi(\mathbf{r}, t) \rangle = 0$ and $\langle \xi(\mathbf{r}, t) \xi(\mathbf{r}', t') \rangle \sim \delta(\mathbf{r} - \mathbf{r}') \delta(t - t')$. For the OPO case, the diffusion coefficients D_x , D_y , and non-linear coefficients λ_x , λ_y , depend in a non-trivial way on the physical parameters of the system (i.e. g , κ , f_p , k_p , ω_p).

Without vortices, the KPZ equation leads to an algebraic decay of the spatial correlations of θ , i.e. $\langle (\theta(\mathbf{R} + \mathbf{r}, t) - \theta(\mathbf{R}, t))^2 \rangle \sim \tilde{r}^{2\chi}$, where \tilde{r} is the distance rescaled to take into account the anisotropy, $\tilde{r}^2 = (x/x_0)^2 + (y/y_0)^2$, and $\chi \approx 0.39$ [32–34] is a universal critical exponent for 2D KPZ. Under the assumption that we can neglect the effect of density fluctuations, these phase correlations would result in the spacial correlations of the momentum-filtered signal field $\Psi_s(\mathbf{x}, t)$ showing a stretched exponential decay with distance $g_s^{(1)}(\mathbf{r}) \sim e^{-\tilde{r}^{2\chi}}$ [26].

Finding the ideal pump strength for observing the KPZ. In Ref. [26], it was shown that within certain bounds in pump strength f_p , the non-linearity of the KPZ equation corresponding to the polariton OPO system can become large enough that the characteristic stretched exponential decay of spatial correlations should become observable at all length scales. While this range in f_p is known roughly from the previous results [26], it ultimately depends on the exact value of the signal momentum, which

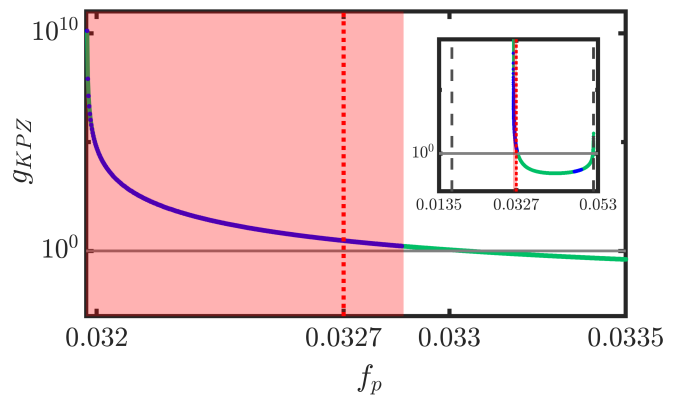


FIG. 2. KPZ non-linearity g_{KPZ} as a function of the pump strength, f_p . The blue line shows where the three-mode ansatz, assumed in deriving the KPZ equation for OPO, is stable. The window where we expect stretched exponential decay at all length scales is given by $g_{KPZ} \geq 1$ (horizontal line marks $g_{KPZ} = 1$). The red shaded region shows where both three-mode OPO is stable and $g_{KPZ} \geq 1$. The dotted vertical red line marks $f_p = 0.0327$, which we have chosen as representative for full numerical analysis. Parameters are $k_p = 1.4$, $k_s = 0.2084$, $\gamma = 0.045$, $\hbar\Omega_R = 4.4\text{meV}$, as in numerical simulations (k_s is chosen to match that seen in the numerics at $f_p = 0.0327$). Inset shows the full range of f_p where OPO occurs, with the dashed vertical lines marking the OPO thresholds for our value of k_s .

is not an externally controlled parameter but is chosen by the system as the OPO state forms, often in a way that is difficult to predict analytically [27]. As a result the first step is to test the behaviour at a selection of pump strengths around where we expect the window to be, and then check where the exact window is for the signal momentum that occurs at those pump strengths, and that the chosen f_p actually falls within it. Figure 2 shows the KPZ non-linearity g_{KPZ} (as defined in the analysis in [26]) as a function of f_p for the signal momentum found in the example cases. The window where stretched exponential decay is expected to be visible is for where g_{KPZ} is defined and ≥ 1 .

Numerical results. To begin with, we investigate how the behaviour within the KPZ window, which we choose to examine at $f_p = 0.0327$, differs from that outside it. In fig. 3 we compare correlations along the x and y directions for three different values of f_p , one within the window, as mentioned at $f_p = 0.0327$, and one outside the window on either side, $f_p = 0.026$ in the middle of the OPO region and $f_p = 0.051$ near the upper threshold.

A number of distinct differences between the behaviour inside and outside the KPZ window are already recognisable just from inspection. Firstly, within the window $g_s^{(1)}(\mathbf{r})$ decays much faster with distance in both directions. This is consistent with signatures of KPZ physics becoming apparent within this window, as the stretched exponential decay is faster than the algebraic decay of

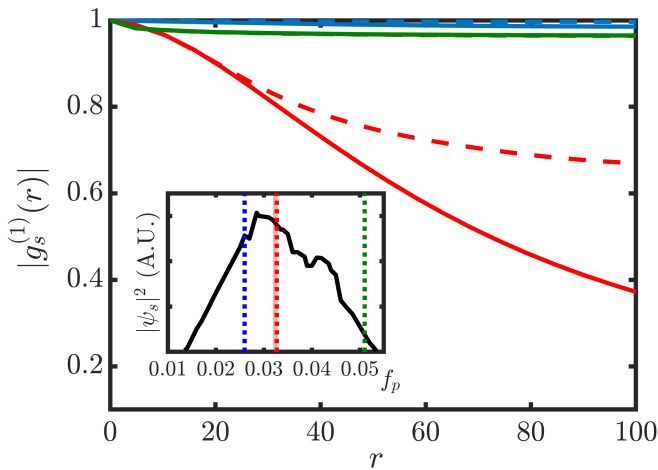


FIG. 3. Comparison of $g_s^{(1)}(\mathbf{r})$ at different pump strengths f_p for \mathbf{r} taken along the x (dashed lines) or y (solid lines) directions. For $f_p = 0.0327$ (red lines), within the KPZ window (shaded red in Fig. 2), correlations decay significantly faster, and with stronger anisotropy, than $f_p = 0.026$ (blue lines) and $f_p = 0.051$ (green lines) on either side of the window. Inset: Signal density versus pump strength f_p , vertical dotted lines indicate the chosen example values.

correlations previously observed in polariton OPO [25]. Note, that the quasi-condensate density of the signal at the pump strength chosen inside the KPZ window (marked by red dotted vertical line in Fig. 3) is actually significantly larger than at the considered pump strengths outside of the KPZ window (marked by blue and especially by green dotted vertical line in Fig. 3). In the usual case of algebraic decay of correlations associated with the quasi-ordered state in two dimensions [25], lower densities always mean faster decay of coherence. In fact here, the blue and green lines in Fig. 3 are so far away from the BKT transition that we observe almost constant $g_s^{(1)}(\mathbf{r})$ very close to one indicating a nearly coherent state. The fact that we observe a much faster decay of correlations for a case with significantly larger signal density than for cases with much lower densities, indicates strongly that the physics is dominated by a different type of fluctuations than in equilibrium 2D quasi-condensates. Curiously, the KPZ window also displays much more significant anisotropy in the behaviour of $g_s^{(1)}(\mathbf{r})$; outside the window the decay of correlations is almost independent of the direction, while inside it the correlations decay much more with distance in the y direction than in x .

Fitting the form of spatial correlations. With a clear indication that something significant is occurring within the KPZ window, we now investigate whether it is indeed caused by KPZ fluctuations i.e. how well this behaviour fits to the stretched exponential form predicted by the KPZ equation. For this purpose we fit the form of $g_s^{(1)}(\mathbf{r})$ to three different models: algebraic decay

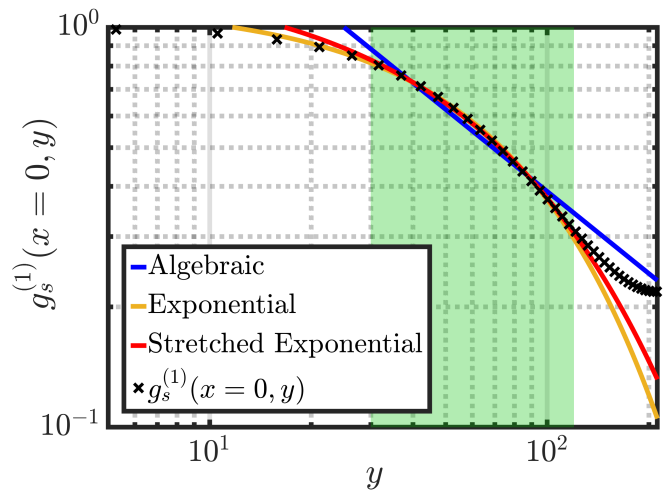


FIG. 4. $g_s^{(1)}(x=0, y)$ with fits to algebraic (blue), exponential (yellow), and stretched exponential (red) decay. Green shaded region indicates the points included in the fit.

($g_s^{(1)}(r) \sim r^{-\alpha}$), exponential decay ($g_s^{(1)}(r) \sim e^{-\frac{r}{\tau_0}}$), and stretched exponential decay (as defined above) with the universal exponent $\chi = 0.39$.

For the case $f_p = 0.0327$, correlations in the y direction fit well to the stretched exponential decay. In fig. 4 we show the algebraic, exponential, and stretched exponential fits to $g_s^{(1)}(x=0, y)$ for $f_p = 0.0327$. For the fits we exclude both the short range behaviour, which is not expected to obey the stretched exponential form that is found in the long-range limit, and the furthest points that are most significantly affected by the finite size of the system and periodic boundary conditions. Further discussion of the exact justification of our fitting bounds is included in the supplementary material. For this central portion of the correlation function, the stretched exponential decay fits significantly better than the algebraic decay, which would be expected in the case we did not have KPZ physics, and slightly better than the pure exponential decay also. Additionally, we do not expect a pure exponential decay of correlations since this is associated with strong disorder, i.e. for our type of system, the presence of vortices, and we do not find any vortices in the momentum-filtered signal field $\Psi_s(\mathbf{x}, t)$. As indicated earlier, our case is far away from the BKT transition and deep in the quasi-condensate phase, where without the KPZ type fluctuations we would expect the usual slow algebraic decay of correlations. Fig. 5 shows clearly the crossover from the Gaussian decay of correlations at short range to the stretched exponential decay of correlations within our fitting bounds, that is indicative of the expected KPZ behaviour in the “long-range limit”.

It is not entirely clear why the correlations in x direction do not match as well to the stretched exponential decay. A possible explanation may be the effect of additional satellite modes (arranged along k_x), which are

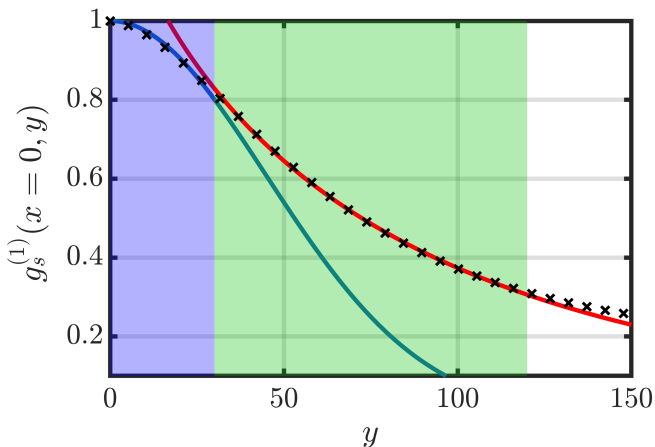


FIG. 5. $g_s^{(1)}(x=0, y)$ showing fits to Gaussian form (blue line) of short range correlations at $y < 30$ (blue shaded region) and the fit to stretched exponential decay with $\chi = 0.39$ (red line) in the (green shaded) region $30 < y < 120$.

not accounted for in the analytical mapping from polariton OPO to KPZ equation, and may lead to additional effects.

Summary and Outlook. We have shown that the signatures of KPZ fluctuations in polariton OPO can be seen clearly in the numerical solution of the system's microscopic equations of motion. Although we do observe additional complexity, such as the effects of satellite states, compared to the three mode analytical model used to predict this behaviour [26], the characteristic stretched exponential decay of first order spatial correlations is still clearly visible in the direction perpendicular to the pump momentum. Furthermore, the dramatic change in the form of spatial correlations seen when the pump strength is tuned to within the window where KPZ behaviour is expected at all length scales, suggests that this regime should be easy to distinguish despite the small range of pump strengths for which it occurs. Overall, our work strongly suggests the viability of polariton OPO in semiconductor microcavities as an experimental platform for realising and exploring KPZ physics in two dimensions, and gives an indication of how the parameters of such a system may be chosen in order to achieve this.

We gratefully acknowledge financial support from QuantERA InterPol and EPSRC (Grant No. EP/R04399X/1 and No. EP/K003623/2).

-
- [1] M. Kardar, G. Parisi, and Y.-C. Zhang, Dynamic scaling of growing interfaces, *Phys. Rev. Lett.* **56**, 889 (1986).
 [2] T. Vicsek, M. Cserz, and V. K. Horvth, Self-affine growth of bacterial colonies, *Physica A: Statistical Mechanics and its Applications* **167**, 315 (1990).

- [3] J. ichi Wakita, H. Itoh, T. Matsuyama, and M. Matsushita, "self-affinity for the growing interface of bacterial colonies", *Journal of the Physical Society of Japan* **66**, 67 (1997).
 [4] M. A. C. Huergo, M. A. Pasquale, A. E. Bolzán, A. J. Arvia, and P. H. González, Morphology and dynamic scaling analysis of cell colonies with linear growth fronts, *Phys. Rev. E* **82**, 031903 (2010).
 [5] J. Maunuksela, M. Mylly, O.-P. Kähkönen, J. Timonen, N. Provatas, M. J. Alava, and T. Ala-Nissila, Kinetic roughening in slow combustion of paper, *Phys. Rev. Lett.* **79**, 1515 (1997).
 [6] M. Mylly, J. Maunuksela, M. Alava, T. Ala-Nissila, J. Merikoski, and J. Timonen, Kinetic roughening in slow combustion of paper, *Phys. Rev. E* **64**, 036101 (2001).
 [7] L. Miettinen, M. Mylly, J. Merikoski, and J. Timonen, Experimental determination of kpz height-fluctuation distributions, *Eur. Phys. J. B* **46**, 55 (2005).
 [8] K. A. Takeuchi, M. Sano, T. Sasamoto, and H. Spohn, "growing interfaces uncover universal fluctuations behind scale invariance", *Sci. Rep.* **1**, 10.1038/srep00034 (2011).
 [9] K. A. Takeuchi and M. Sano, Evidence for geometry-dependent universal fluctuations of the kardar-parisi-zhang interfaces in liquid-crystal turbulence, *Journal of Statistical Physics* **147**, 853 (2012).
 [10] Y. T. Fukai and K. A. Takeuchi, Kardar-parisi-zhang interfaces with curved initial shapes and variational formula, *Phys. Rev. Lett.* **124**, 060601 (2020).
 [11] E. Altman, L. M. Sieberer, L. Chen, S. Diehl, and J. Toner, Two-dimensional superfluidity of exciton polaritons requires strong anisotropy, *Physical Review X* **5**, 011017 (2015).
 [12] K. Ji, V. N. Gladilin, and M. Wouters, Temporal coherence of one-dimensional nonequilibrium quantum fluids, *Phys. Rev. B* **91**, 045301 (2015).
 [13] L. He, L. M. Sieberer, E. Altman, and S. Diehl, Scaling properties of one-dimensional driven-dissipative condensates, *Phys. Rev. B* **92**, 155307 (2015).
 [14] L. M. Sieberer, M. Buchhold, and S. Diehl, Keldysh field theory for driven open quantum systems, *Reports on Progress in Physics* **79**, 096001 (2016).
 [15] G. Wachtel, L. M. Sieberer, S. Diehl, and E. Altman, Electrodynamic duality and vortex unbinding in driven-dissipative condensates, *Phys. Rev. B* **94**, 104520 (2016).
 [16] L. M. Sieberer, G. Wachtel, E. Altman, and S. Diehl, Lattice duality for the compact kardar-parisi-zhang equation, *Phys. Rev. B* **94**, 104521 (2016).
 [17] J. Keeling, L. M. Sieberer, E. Altman, L. Chen, S. Diehl, and J. Toner, Superfluidity and phase correlations of driven dissipative condensates, *ArXiv* (2016), book Chapter, preprint, [arXiv:1601.04495](https://arxiv.org/abs/1601.04495).
 [18] L. He, L. M. Sieberer, and S. Diehl, Space-time vortex driven crossover and vortex turbulence phase transition in one-dimensional driven open condensates, *Phys. Rev. Lett.* **118**, 085301 (2017).
 [19] D. Squizzato, L. Canet, and A. Minguzzi, Kardar-parisi-zhang universality in the phase distributions of one-dimensional exciton-polaritons, *Phys. Rev. B* **97**, 195453 (2018).
 [20] Q. Mei, K. Ji, and M. Wouters, Spatiotemporal scaling of two-dimensional nonequilibrium exciton-polariton systems with weak interactions, *ArXiv* (2020), preprint, [arXiv:2002.01806](https://arxiv.org/abs/2002.01806).

- [21] L. M. Sieberer and E. Altman, Topological defects in anisotropic driven open systems, *Phys. Rev. Lett.* **121**, 085704 (2018).
- [22] A. Zamora, N. Lad, and M. H. Szymańska, Vortex dynamics in a compact kardar-parisi-zhang system, *ArXiv* (2020), preprint, [arXiv:2003.01743](https://arxiv.org/abs/2003.01743).
- [23] V. N. Gladilin and M. Wouters, Vortices in nonequilibrium photon condensates, *ArXiv* (2020), preprint, [arXiv:2006.11095](https://arxiv.org/abs/2006.11095).
- [24] D. Caputo, D. Ballarini, G. Dagvadorj, C. Sanchez Muoz, M. De Giorgi, L. Dominici, K. West, L. N. Pfeiffer, G. Gigli, F. P. Laussy, and et al., Topological order and thermal equilibrium in polariton condensates, *Nature Materials* **17**, 145151 (2017).
- [25] G. Dagvadorj, J. M. Fellows, S. Matyjaśkiewicz, F. M. Marchetti, I. Carusotto, and M. H. Szymańska, Nonequilibrium phase transition in a two-dimensional driven open quantum system, *Phys. Rev. X* **5**, 041028 (2015).
- [26] A. Zamora, L. M. Sieberer, K. Dunnett, S. Diehl, and M. H. Szymańska, Tuning across universalities with a driven open condensate, *Phys. Rev. X* **7**, 041006 (2017).
- [27] K. Dunnett, A. Ferrier, A. Zamora, G. Dagvadorj, and M. H. Szymańska, Properties of the signal mode in the polariton optical parametric oscillator regime, *Phys. Rev. B* **98**, 165307 (2018).
- [28] D. M. Whittaker, Effects of polariton-energy renormalization in the microcavity optical parametric oscillator, *Phys. Rev. B* **71**, 115301 (2005).
- [29] I. Carusotto and C. Ciuti, Quantum fluids of light, *Rev. Mod. Phys.* **85**, 299 (2013).
- [30] I. Carusotto and C. Ciuti, Spontaneous microcavity-polariton coherence across the parametric threshold: Quantum monte carlo studies, *Phys. Rev. B* **72**, 125335 (2005).
- [31] L. M. Sieberer, S. D. Huber, E. Altman, and S. Diehl, Non-equilibrium functional renormalization for driven-dissipative Bose-Einstein condensation, *Phys. Rev. B* **89**, 134310 (2014).
- [32] T. Halpin-Healy and G. Palasantzas, Universal correlators and distributions as experimental signatures of (2 + 1)-dimensional kardar-parisi-zhang growth, *EPL (Europhysics Letters)* **105**, 50001 (2014).
- [33] V. G. Miranda and F. D. A. Aarão Reis, Numerical study of the kardar-parisi-zhang equation, *Phys. Rev. E* **77**, 031134 (2008).
- [34] A. Pagnani and G. Parisi, Numerical estimate of the kardar-parisi-zhang universality class in (2+1) dimensions, *Phys. Rev. E* **92**, 010101(R) (2015).

Supplementary material for: Searching for the Kardar-Parisi-Zhang phase in microcavity polaritons

A. Ferrier,¹ A. Zamora,¹ G. Dagvadorj,¹ and M. H. Szymaska¹

¹*Department of Physics and Astronomy, University College London, Gower Street, London, WC1E 6BT, United Kingdom*

CONVERGENCE CHECKS

To ensure the validity of our findings, we check convergence of the results in time (convergence to steady state), the number of stochastic realisations used, and system size. Additionally, since our fitting involves excluding points beyond certain upper and lower bounds, in order to eliminate short range and edge effects, we check how the results obtained depend on the choice of these bounds.

Convergence to Steady State

We use the mean-field steady-state as the initial condition for our stochastic dynamics. Our prior analysis of stochastic simulations for the OPO system [1] close to the BKT transition showed that the steady-state does not depend on the initial conditions. Different observables can take different times to reach a steady state, with $g_s^{(1)}(\mathbf{r})$ being one of the slowest to converge. Fig. 1 shows the evolution of $g_s^{(1)}(x=0, y)$ in time. Beyond around $t = 120000$, $g_s^{(1)}(x=0, y)$ stops drifting and remains stable except for small fluctuations. All other results are therefore obtained by averaging over the steady state from $t = 120000$ to $t = 160000$.

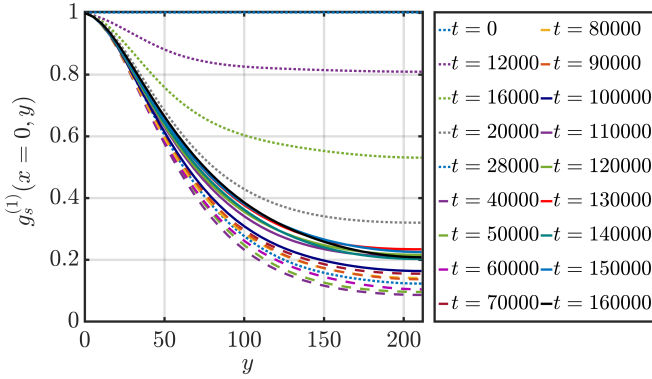


FIG. 1. Calculated $g_s^{(1)}(x=0, y)$ at different times from $t = 0$ to $t = 160000$.

Convergence with number of realisations

Since results from the TWA method are produced by averaging over stochastic realisations, it is important to check that we have used enough realisations to sufficiently sample the underlying distribution, and hence give results that do not depend on the exact number of realisation used. Different physical quantities require different numbers of realisations to converge; for example, the momentum distributions $|\Psi(\mathbf{k}, t)|^2$ can often show minimal differences between individual realisations, but the correlation function $g_s^{(1)}(\mathbf{r})$ typically requires a large number of realisations to fully converge. We used a total of 400 realisations for the main result at $f_p = 0.0327$. To check that this is sufficient we compare the form of $g_s^{(1)}(\mathbf{r})$ when calculated with specific numbers of realisations (see Fig. 2). We see that beyond 300 realisations the form of $g_s^{(1)}(\mathbf{r})$ does not change significantly, suggesting that the 400 realisations is sufficient for capturing the behaviour of correlations.

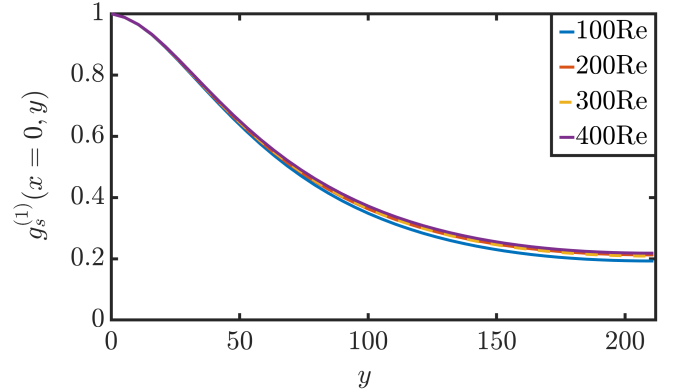


FIG. 2. Calculated $g_s^{(1)}(x=0, y)$ for different numbers of realisations used between 100 and 400. Each case is also time averaged over the steady state.

Convergence with system size

To check that our results do not depend on the system size, we run the simulations again for a slightly smaller system with $N = 386$, $L = 165.85464$. Note that the specific values of N and L are chosen such as to make sure that the signal momentum $k_s = 0.2084$ chosen by

the larger system, still lies on the numerical grid in momentum space for the smaller system, as the calculated KPZ non-linearity shown in Fig. 2 of the main paper is generally dependant on the exact value of k_s , and so we must allow for it to remain the same to truly compare different system sizes.

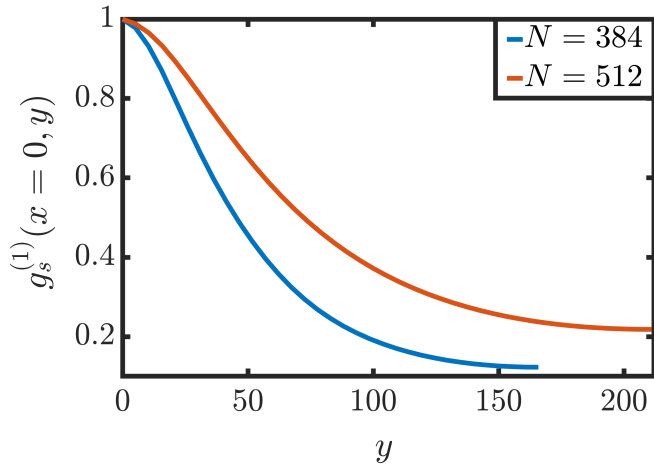


FIG. 3. Calculated $g_s^{(1)}(x=0, y)$ for different system sizes $N = 512$ ($L = 211.08772$, blue line) and $N = 386$ ($L = 165.85464$, red line). Each case is also time averaged over the steady state.

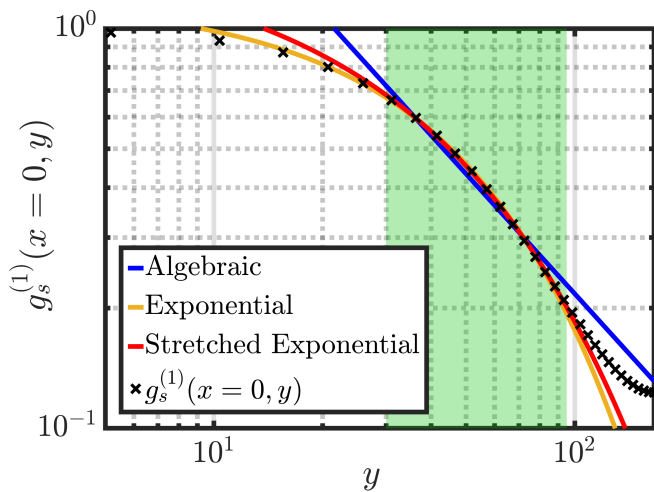


FIG. 4. $g_s^{(1)}(x=0, y)$ with fits to algebraic (blue line), exponential (yellow line), and stretched exponential (red line) decay, for smaller system size ($N = 384$). Green shaded region indicates the points included in the fit.

Although $g_s^{(1)}(x=0, y)$ for the different system sizes differs in magnitude (see Fig. 3), as can be seen from Fig. 4 (for $N = 384$) and Fig. 4 of the main paper (for $N = 512$), both system sizes are independently seen to have a good fit to the stretched exponential decay with exponent $\chi = 0.39$, as predicted from KPZ physics. This suggests that while the exact form of the OPO produced

may still be too finely dependent on the geometry of the system for the sizes we consider, the observability of the signature of KPZ fluctuations is much less dependent on the system size.

Choice of fitting bounds

Here we look at how we choose the exclusion bounds for the points included in our fitting, and how it affects the results of the stretched exponential fit. These exclusions are needed to account for microscopic and boundary effects. Firstly, a lower bound to the fitted region is necessary because the mapping from polariton OPO to the KPZ equation is only valid in the long range limit. The form of the correlations at short distances is not universal and may depend on the microscopic details of the specific system. The upper fitting bound instead solves a problem of a more practical origin: the finite size of the simulated system, and the boundary conditions imposed at the edges of that finite system. For the simulations we use periodic boundary conditions, which tend to enhance the correlations near the edges.

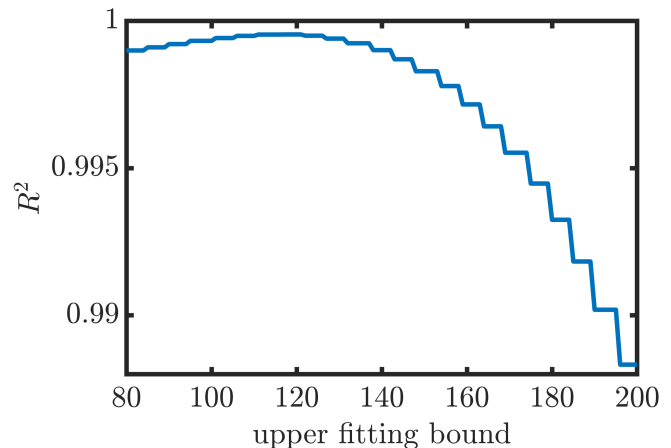


FIG. 5. Coefficient of determination R^2 for stretched exponential fit and a function of the chosen upper fitting bound. Lower fitting bound is fixed as $y > 30$.

As shown in Fig. 5 of the main paper, we can justify our choice of lower bound by fitting the expected Gaussian form of the short range correlations. We see that $g_s^{(1)}(x=0, y)$ fits well to a Gaussian form for $y < 30$, and so choose to exclude points with $y < 30$ from our fits for the long range form of the correlations. The appropriate upper fitting bound is a bit harder to determine robustly. In practice, we should exclude the area which is affected by the periodic boundary conditions i.e. where the correlations start to grow due to the proximity of the next unit cell. However, as we can see in Fig. 5, the quality of our stretched exponential fit, as given by the coefficient of determination R^2 does not depend strongly on

our choice of upper bound until around $y = 140$, beyond which it begins to fall much more rapidly. We therefore feel comfortable choosing to exclude points with $y > 120$ from our stretched exponential fit (which maximises R^2) to remove the edge effects, knowing that while the choice is somewhat arbitrary, it does not significantly affect our results.

-
- [1] G. Dagvadorj, J. M. Fellows, S. Matyjaśkiewicz, F. M. Marchetti, I. Carusotto, and M. H. Szymańska, Nonequilibrium phase transition in a two-dimensional driven open quantum system, *Phys. Rev. X* **5**, 041028 (2015).